The Astrophysical Journal, 834:45 (7pp), 2017 January 1 doi:10.3847/1538-4357/834/1/45

STRONG LENSING ANALYSIS OF THE GALAXY CLUSTER MACS J1319.9+7003 AND THE DISCOVERY OF A SHELL GALAXY

Adi Zitrin[1,2,3]
[1] Cahill Center for Astronomy and Astrophysics, California Institute of Technology, MC 249-17, Pasadena, CA 91125, USA; adizitrin@gmail.com
[2] Physics Department, Ben-Gurion University of the Negev, P.O. Box 653, Béer-Sheva 84105, Israel
Received 2016 September 2; revised 2016 October 28; accepted 2016 November 6; published 2016 December 29

ABSTRACT

We present a strong-lensing (SL) analysis of the galaxy cluster MACS J1319.9+7003 ($z = 0.33$, also known as Abell 1722), as part of our ongoing effort to analyze massive clusters with archival *Hubble Space Telescope* (*HST*) imaging. We spectroscopically measured with Keck/Multi-Object Spectrometer For Infra-Red Exploration (MOSFIRE) two galaxies multiply imaged by the cluster. Our analysis reveals a modest lens, with an effective Einstein radius of $\theta_e(z = 2) = 12 \pm 1''$, enclosing $2.1 \pm 0.3 \times 10^{13}\ M_{\odot}$. We briefly discuss the SL properties of the cluster, using two different modeling techniques (see the text for details), and make the mass models publicly available (ftp://wise-ftp.tau.ac.il/pub/adiz/MACS1319/). Independently, we identified a noteworthy, young shell galaxy (SG) system forming around two likely interacting cluster members, $20''$ north of the brightest cluster galaxy. SGs are rare in galaxy clusters, and indeed, a simple estimate reveals that they are only expected in roughly one in several dozen, to several hundred, massive galaxy clusters (the estimate can easily change by an order of magnitude within a reasonable range of characteristic values relevant for the calculation). Taking advantage of our lens model best-fit, mass-to-light scaling relation for cluster members, we infer that the total mass of the SG system is $\sim 1.3 \times 10^{11}\ M_{\odot}$, with a host-to-companion mass ratio of about 10:1. Despite being rare in high density environments, the SG constitutes an example to how stars of cluster galaxies are efficiently redistributed to the intra-cluster medium. Dedicated numerical simulations for the observed shell configuration, perhaps aided by the mass model, might cast interesting light on the interaction history and properties of the two galaxies. An archival *HST* search in galaxy cluster images can reveal more such systems.

Key words: galaxies: clusters: general – galaxies: clusters: individual (MACS J1319.9+7003 – Abell 1722) – galaxies: evolution – galaxies: formation

1. INTRODUCTION

Shell galaxies (SGs) are typically elliptical galaxies surrounded by low surface brightness shells, or at times cones seen as concentric arcs around the SG center. The first SGs were noted some 50–60 years ago (Arp 1966, see also Zwicky 1956), and then in earnest around the early 1980s (Malin & Carter 1980), and have been then studied observationally, analytically, and by numerical simulations (e.g., Malin & Carter 1983; Quinn 1984; Athanassoula & Bosma 1985; Schweizer & Ford 1985; Dupraz & Combes 1986; Hernquist & Quinn 1988, and references therein). Significantly improved computer power in recent years has become particularly useful for simulating such galaxies with greater detail (e.g., Cooper et al. 2011; Ebrová et al. 2012; Ebrova 2013), generating renewed interest in these systems (see also Canalizo et al. 2007; Sikkema et al. 2007; Bennert et al. 2008; Foster et al. 2014).

The shells are a particular tidal feature that forms as a result of an interaction between two galaxies (for a recent review of SGs, see Ebrova 2013 and references therein), in particular a highly radial, minor merger (Quinn 1984, but see also Hernquist & Spergel 1992). The shells consist of stars stripped by the interaction, oscillating in the system's potential well and forming faint envelopes near the turnaround radii (e.g., Dupraz & Combes 1986; Hernquist & Quinn 1988). Shells are relatively common around elliptical galaxies (at least 10% show shells, e.g., Malin & Carter 1983; Athanassoula & Bosma 1985; Ebrova 2013), but are quite rare around spiral or disk galaxies (cf. Schweizer & Seitzer 1988; Fardal et al. 2007; Foster et al. 2014). Despite being seen mostly around elliptical galaxies, most shells have been observed in the field rather than in clusters of galaxies (e.g., Malin & Carter 1983; Athanassoula & Bosma 1985). This is likely a result of various factors, primarily the low cross-section for small impact parameter galaxy encounters within the cluster ($\pi r_{\rm core}^2$, where $r_{\rm core}$ is the typical galaxy's core size), the collisionlessness of dark matter and stars, combined with high encounter velocities which lower the chances for merger within the cluster. In addition, it is conceivable the intra-cluster light may also play a role in smoothing the shell structure in clusters so it becomes harder to observe due to lack of contrast.

The number of shells and distance between them can shed light on the interaction or merger history of the two galaxies, as in each passage of the smaller galaxy at the host's center (Gu et al. 2013), more material is stripped to form an expanding front (e.g., Quinn 1984; Ebrova 2013). The shape of the shell, especially in the case of narrow cones, adds useful information that can be then used to tighten the constraints on the initial configuration, relative masses, and velocities (Hernquist & Quinn 1988; Ebrová et al. 2012), although significant degeneracies exist. Also, color information and gradients, if seen, might add information relevant for a population synthesis of the shell stars and the system's history (e.g., Sikkema et al. 2007; Bílek et al. 2016).

Here, we present an SG system caught relatively early on, so that only one highly symmetric shell is seen on each side of the system, where the distance of the shell on one side is half the distance on the other side, and the two interacting galaxies are

[3] Hubble Fellow.

both still observed (see also Bílek et al. 2016). The SG is formed in a massive galaxy cluster, MACS J1319.9+7003 (hereafter M1319, $z = 0.33$; Ebeling et al. 2010; Mantz et al. 2010; also known as Abell 1722; Abell et al. 1989), where, as mentioned, SGs are generally considered less common.

The system was identified in the framework of our ongoing effort (e.g., Zitrin & Broadhurst 2016) to lens-model massive clusters with available *Hubble Space Telescope* (*HST*) imaging, toward the launch of the *James Webb Space Telescope* (*JWST*). Since one of the main goals of *JWST* is to target galaxies in the era of reionization, strong lensing (SL) by galaxy clusters will be of increasing importance for detecting the faintest, highest-redshift galaxies. In addition, M1319 has another interesting aspect due to its high ecliptic latitude, where both the infrared (IR) background is ∼1.3 mag fainter (Windhorst et al. 2011) and dust extinction from our Galaxy is minimized, so it may become a good candidate for high-redshift searches in the future. Here we map the projected mass distribution of M1319, from measurements of two strongly lensed galaxies we identify and measure below. The model is made publicly available for future studies of matter distributions in clusters (Meneghetti et al. 2014; Donahue et al. 2016; Umetsu et al. 2016), lensed background sources or lensing-efficiency measurements (Coe et al. 2015; Lotz et al. 2016), but also, if so desired, it can be used to numerically simulate the details and environment of the SG with greater detail.

The presented SG, although rare, supplies an interesting example of how galaxies can merge, evolve, and lose their material to the intra-cluster medium (e.g Edwards et al. 2016), warranting further study (see also Gu et al. 2013). However, despite the interesting case of the SG, note that we will only present and give its basic characteristics, and the paper mainly concentrates on the SL properties of the cluster, so that we leave a detailed examination (and possibly numerical simulation) of the SG system to other dedicated work.

The paper is organized as follows. In Section 2 we review the different observations, and show the spectra of the identified multiply imaged galaxies. In Section 3 we construct a mass model for the cluster and summarize its properties. In Section 4 we summarize and discuss the results, including an estimate of the occurrence of SGs in galaxy clusters. Throughout we use a standard Lambda-cold dark matter (ΛCDM) cosmology with $\Omega_{m0} = 0.3$, $\Omega_{\Lambda 0} = 0.7$, $H_0 = 100\,h\,\mathrm{km\,s^{-1}\,Mpc^{-1}}$, $h = 0.7$, and magnitudes are given using the AB convention. $1''$ equals 4.75 kpc at the redshift of the cluster, $z_l = 0.33$. Unless noted otherwise, errors are 1σ.

2. DATA AND OBSERVATIONS

We primarily use archival *HST* observations of the galaxy cluster M1319, in which we identified the lensed features and noted the SG. These data include imaging in four bands from *HST* programs 10266 and 10491 (PI: Ebeling) available through the Hubble Legacy Archive: a F606W image (total exposure time 1200 s), taken on 2005 November 04, and a F814W image (total exposure time 1440 s), taken on 2011 January 22, with the ACS/WFC; and F110W and F140W, 705.88 s each, taken on 2011 July 17 with the WFC3/IR.

We ran SExtractor (Bertin & Arnouts 1996) in dual-mode to obtain the photometry of objects in the cluster field, useful for identifying multiply imaged galaxies as well as red-sequence cluster members (Section 3). We then used the resulting catalogs as input and run the Bayesian Photometric Redshift program (Benítez 2000; Coe et al. 2006) to derive photometric redshifts, especially examining multiple-image candidates.

We observed the cluster field with the Multi-Object Spectrometer For Infra-Red Exploration (MOSFIRE; McLean et al. 2012) on the Keck I telescope, for approximately half an hour, consisting of sets of 120 s exposures, on 2015 June 10, placing a slit along the SG system, and on multiple-images 1.1 and 2.2 seen in Figure 1. Observations were carried out in the H-band, primarily to examine if a prominent Paschen-beta (Paβ) line was present in the SG and to capture redshifted optical or long ultra-violet (long-UV) spectral lines from the multiply imaged systems. We adopted a dither pattern of $\pm 2''$ along the slit.

Data reduction was performed using the official MOSFIRE pipeline.[4] For each flat-fielded slit we extracted the one-dimensional (1D) spectrum using an 11 pixel boxcar ($\simeq 1''$) centered on the target, and a similar procedure was adopted in quadrature to derive the 1σ error distribution. We used two stars with known magnitudes, on which slits were placed in order to track possible drifts, for estimating the absolute depth of our observations. We reached a 3σ flux density limit of $\sim 2.1 \times 10^{-18}\,\mathrm{erg\,cm^{-2}\,s^{-1}\,\AA^{-1}}$ between skylines, which for a marginally resolved line (FWHM = 5 Å line) translates into a 3σ line flux limit of $\sim 1.8 \times 10^{-18}\,\mathrm{erg\,cm^{-2}\,s^{-1}}$, in good agreement with the MOSFIRE exposure time calculator (yielding $3\sigma \sim 2 \times 10^{-18}\,\mathrm{erg\,cm^{-2}\,s^{-1}}$) and with our expectations based on previous observations and taking into account the different exposure times (e.g., Zitrin et al. 2015a). The absolute calibration also agrees to within 10% typically with the nominal MOSFIRE absolute calibration files (C. Steidel, private communication). No prominent lines were detected in the SG slit, disfavoring exotic, active galactic nucleus (AGN)-related mechanisms for the observed cones, such as ionization cones or jet-related features (a typical FWHM of an AGN can often reach order 1000–3000 $\mathrm{km\,s^{-1}}$). This spectrum is thus not shown. The reduced 2D and 1D spectra of multiple images 1.1 and 2.2 are shown in Figure 2, corresponding to $z_s = 1.55$ for system 1, and $z_s = 3.52$ for system 2, although the latter is less certain, as we show and discuss in Figure 2.

3. LENS MODEL

To construct an SL model for M1319 we primarily use the light-traces-mass (LTM) approach by Zitrin et al. (2009; see also Broadhurst et al. 2005; Zitrin et al. 2015b). Full details can be found in these papers. Here we describe the method with brevity.

We start with the cluster galaxies, chosen by following the red-sequence in a color–magnitude diagram. Each member galaxy is parametrized as a power-law mass density distribution, with a weight in proportion to its luminosity, and the superposition of all galaxies makes the total galaxy component of the model. The power-law exponent is the same for all galaxies and is a free parameter of the model. This mass density map is then smoothed with a 2D Gaussian, whose width is also a free parameter of the model, to obtain the smooth dark matter component (this is why this method is referred to as LTM—both the galaxy and dark matter component follow the light). The two components are then combined with a relative weight—the third free parameter of

[4] http://www2.keck.hawaii.edu/inst/mosfire/drp.html

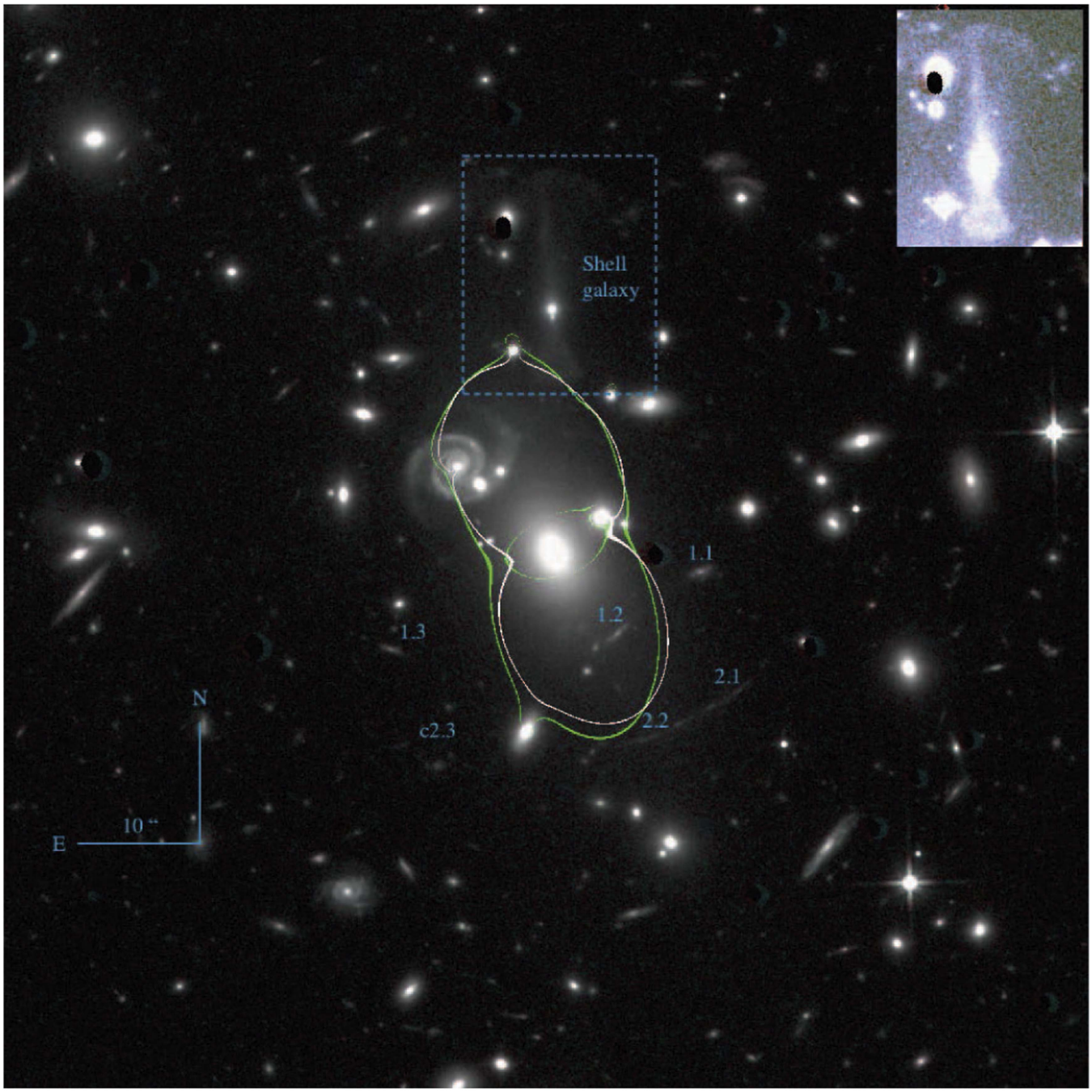

Figure 1. Central field of the galaxy cluster M1319. The SG is marked with a dashed rectangle whose length is $\simeq 20''$ ($1''$ is 4.75 kpc at the cluster's redshift), and is inset as a stamp in the upper-right corner, with higher contrast. The image also shows two sets of multiply imaged galaxies we identified and measured spectroscopically with Keck/MOSFIRE. We constructed two complementary SL models (see text for details) for the cluster using those two systems, excluding image 2.3 (rendered a candidate, less secure identification marked with "c" above). The critical curves from the models are marked in white and green, for a source at redshift $z = 1.55$ (system 1), enclosing an area with an effective Einstein radius of $\theta_e(z = 1.55) = 11 \pm 1''$. The image is constructed from F110W and F140W *HST*/WFC3 imaging (see Section 2).

the method, which along with the overall normalization, brings the number of free parameters to four. A two-parameter external shear is usually also added to allow further flexibility, and to improve the fit further we sometimes allow single bright galaxies to be freely weighted in the minimization and deviate from the nominal mass-to-light ratio adopted (in our case, only the brightest cluster galaxy (BCG) is left to be freely weighted). We also leave the ellipticity of the BCG a free parameter.

We first ran a model fixing the redshift of system 1 to $z = 1.55$ as indicated by our MOSFIRE data (Figure 2), but allowing the redshift of system 2 to vary given the line identification in this system was ambiguous. We ran various models with different priors and found that they place system 2 at $z \sim 3.5$, a noticeably higher redshift than initially implied by its $z \sim 1.6$ [1.2–1.9] photometric redshift. Following the model's preference we searched more carefully for spectroscopic solutions around $z \sim 3.5$ for system 2, and managed to

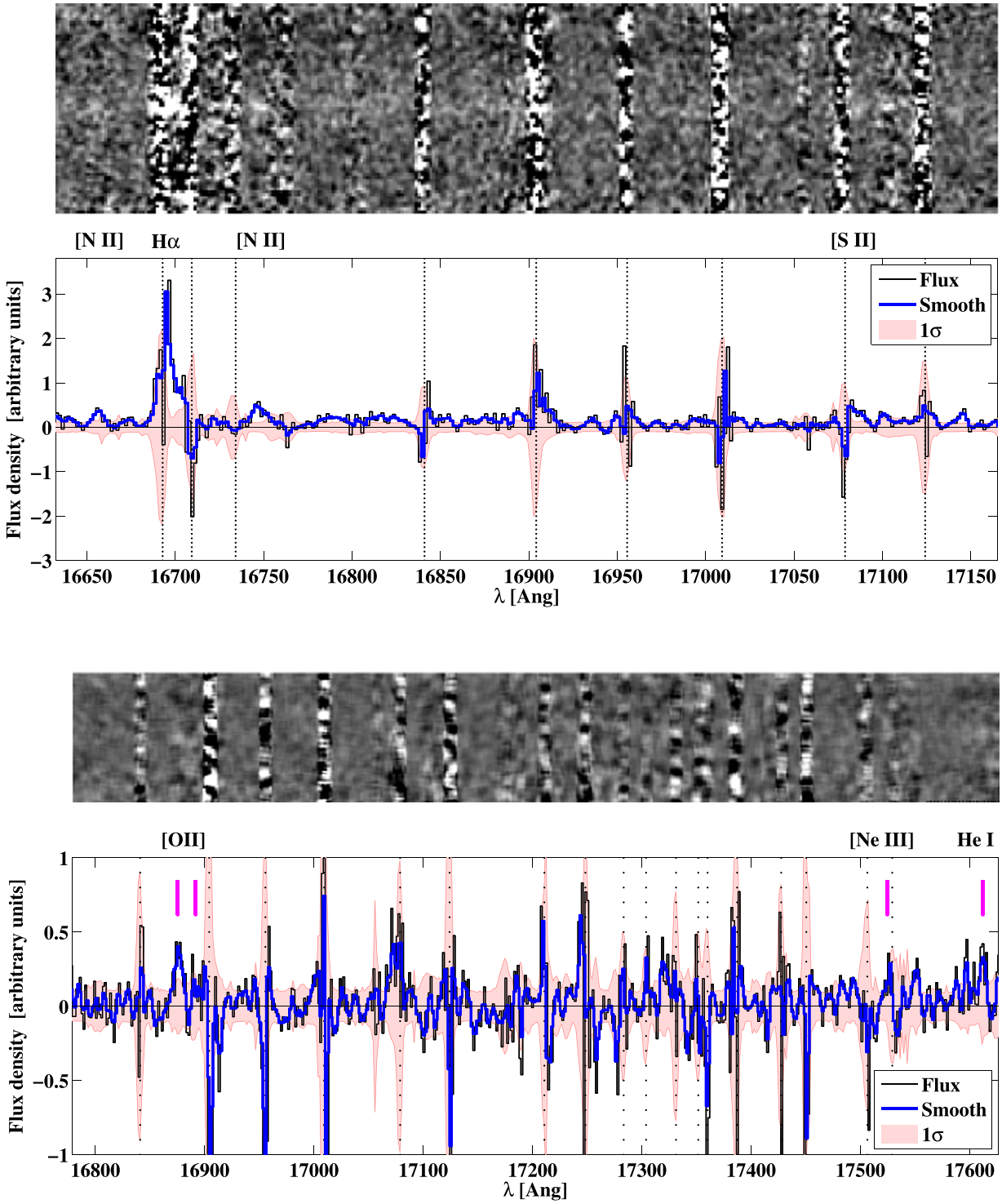

Figure 2. Spectra of multiple images 1.1 (upper subfigure) and 2.2 (bottom subfigure). Each subfigure shows both the 2D (upper inset) and 1D spectra (bottom inset; black curve), including a slightly smoothed version of the 1D spectra for illustrative purposes (blue curve). The 1σ error is also shown as a pink shaded region. In image 1.1 we identify the two [N II] doublet lines ($\lambda\lambda$ 6549,6583 Å) bracketing the prominent Hα line (λ6563 Å), and additionally, the [S II] (λ6717 Å) doublet-line seems to be present as well (the expected position of the other doublet line, [S II] (λ6731 Å), falls on a skyline). These correspond to a redshift of $z = 1.55$ in excellent agreement with the photometric redshift (and 95% C.L.) of 1.44 [1.20–1.68]. Image 2.2 is fainter and line identification is less secure. We utilize the redshift prediction from our lens model, $z \sim 3.4 - 3.6$, to best-fit a redshift of 3.52 following the likely—but tentative—identification of the [O II] doublet ($\lambda\lambda$3726,3729 Å), the He I (λ3889 Å), and [Ne III] (λ3868 Å) lines ([Ne IV] and [Ne V] are also covered in the slit but are not identified). We add purple markers to note the position of these faint lines.

identify the [O II] doublet and other faint lines, seen in the expected position. We thus infer—even if somewhat more tentatively—a redshift of $z = 3.52$ for system 2. We fixed its redshift to this value and reran the model whose resulting critical curves are seen in Figure 1. The minimization of the model included about a couple thousand Monte Carlo Markov Chain steps, and the final LTM model has an image reproduction rms of $0\farcs6$.

We also construct a complementary, fully parametric model using our so-called PIENDeNFW pipeline (see Zitrin et al. 2015b): pseudo-isothermal elliptical mass distributions are used to model the cluster galaxies, scaled by their light (following the prescription of Jullo et al. 2007), and the DM component is an analytic elliptical Navarro–Frenk–White (NFW; Navarro et al. 1996) form. This method is particularly relevant for our case since it adopts well-tested scaling relations (see also Monna et al. 2016) for the cluster galaxies and thus gives an empirical separation between the galaxies and cluster-scale dark components, so that we can estimate directly what is the mass of the SG. The final rms for this model is $\sim 1''$, slightly higher than that of the LTM model.

The two mass distributions and profiles (Figure 3) are in rough agreement—with some differences expected given their different parametrizations and the small number of constraints available. In that sense they can be referred to as preliminary models. Both models however agree well—to within 5%—regarding the size of the lens (see Figure 1): we measure an effective Einstein radius of $\theta_e(z = 1.55) \simeq 11''$ for the redshift of system 1, and $\theta_e(z = 3.52) = 14''$ for that of system 2. The critical curves for these redshifts enclose $\simeq 1.8 \times 10^{13}$ and $\simeq 2.6 \times 10^{13}\ M_\odot$, respectively, and the two models agree to within 10% on these mass measurements. For $z_s = 2$, a value often used for comparison, we find $\theta_e(z = 2) \simeq 12''$ enclosing $\simeq 2.1 \times 10^{13}\ M_\odot$. Note the nominal uncertainties we typically adopt for these quantities are 10% on the Einstein radii and 15% on the enclosed mass. These nominal uncertainties are only slightly higher than the typical statistical uncertainties but encompass better the underlying systematics (Zitrin et al. 2015b).

Note that the final rms of our pipeline is often somewhat higher than in other schemes: the LTM model, and for self-consistency purposes also the fully parametric PIEMDeNFW model, are in practice constructed on a grid, whose resolution is, for speed-up purposes, comparable to or somewhat lower than that of *HST*. In significant magnification regions the round-up of the average source position to the grid's lower resolution pixel scale introduces a finite, non-negligible rms error of order $0.''1$ per system, contributing quite significantly to the global, quoted imprecision of the model (but, importantly, without harming its reliability nor prediction power). These points have been recently emphasized in more length in a community effort to compare lens-modeling techniques to simulated clusters (Meneghetti et al. 2016), and we refer the interested reader to that work for more discussion to this end.[5]

4. DISCUSSION AND SUMMARY

M1319 is a massive galaxy cluster, with an X-ray inferred mass of $M_{500} = 4.8 \pm 0.9 \times 10^{14}\ M_\odot$ (Mantz et al. 2010), and a measured velocity dispersion of $\sim 1000\ \mathrm{km\ s^{-1}}$, in good agreement with its weak-lensing (WL) measurement, suggesting $\sigma_{\rm WL} = 1160 \pm 140\ \mathrm{km\ s^{-1}}$ (Irgens et al. 2002). Naturally, not all massive clusters have SL regions in proportion to their overall mass. To maximize the SL properties, great importance lies in how the matter is distributed within the cluster, for example, its concentration (Broadhurst et al. 2008) and elongation along the line of sight (e.g., Hennawi et al. 2007; Sereno et al. 2010; Merten et al. 2015), or alternatively, if there

[5] Also note we aim to improve this numerically in the near future.

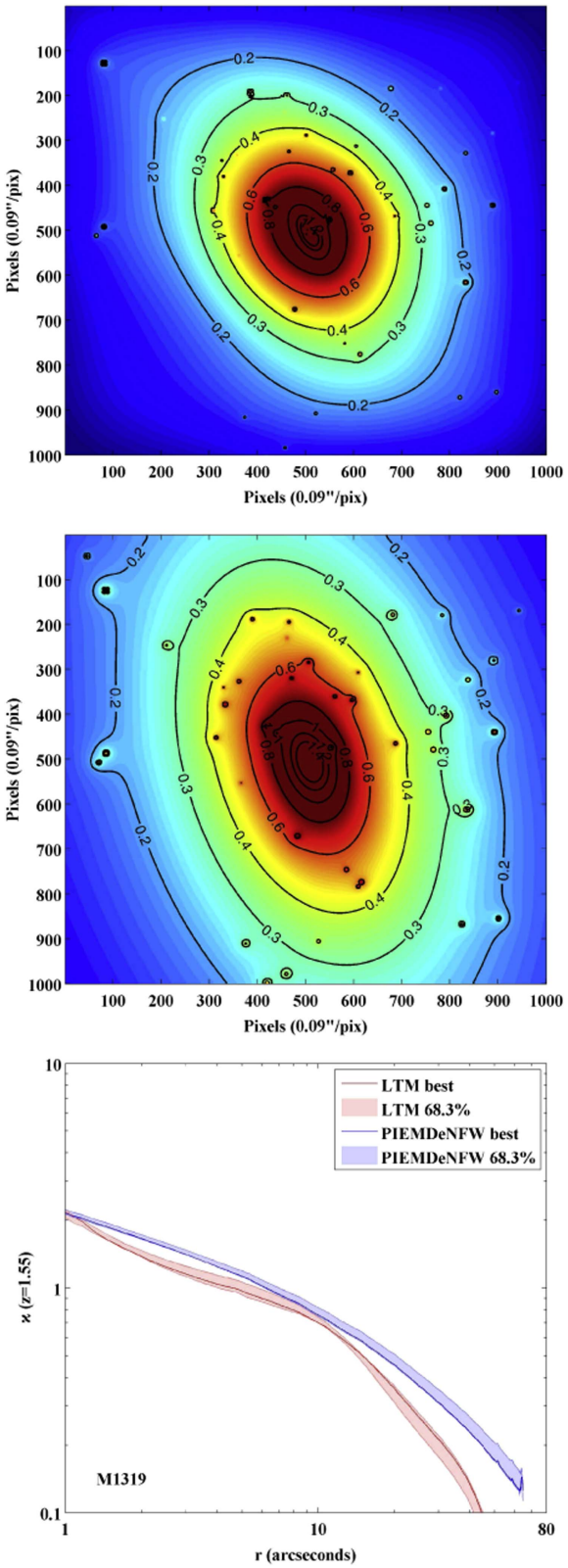

Figure 3. Resulting mass models. The upper panel shows the mass-density *kappa* map for a source at $z_s = 1.55$, the redshift of system 1, for the LTM model; the middle panel for the PIEMDeNFW model; and the bottom panel shows the resulting *kappa* profile from the two models. Some notable differences are seen, which are, however, not surprising given the low number of constraints and different parametrizations. For further discussion on differences between the methods see Zitrin et al. (2015b) and Meneghetti et al. (2016).

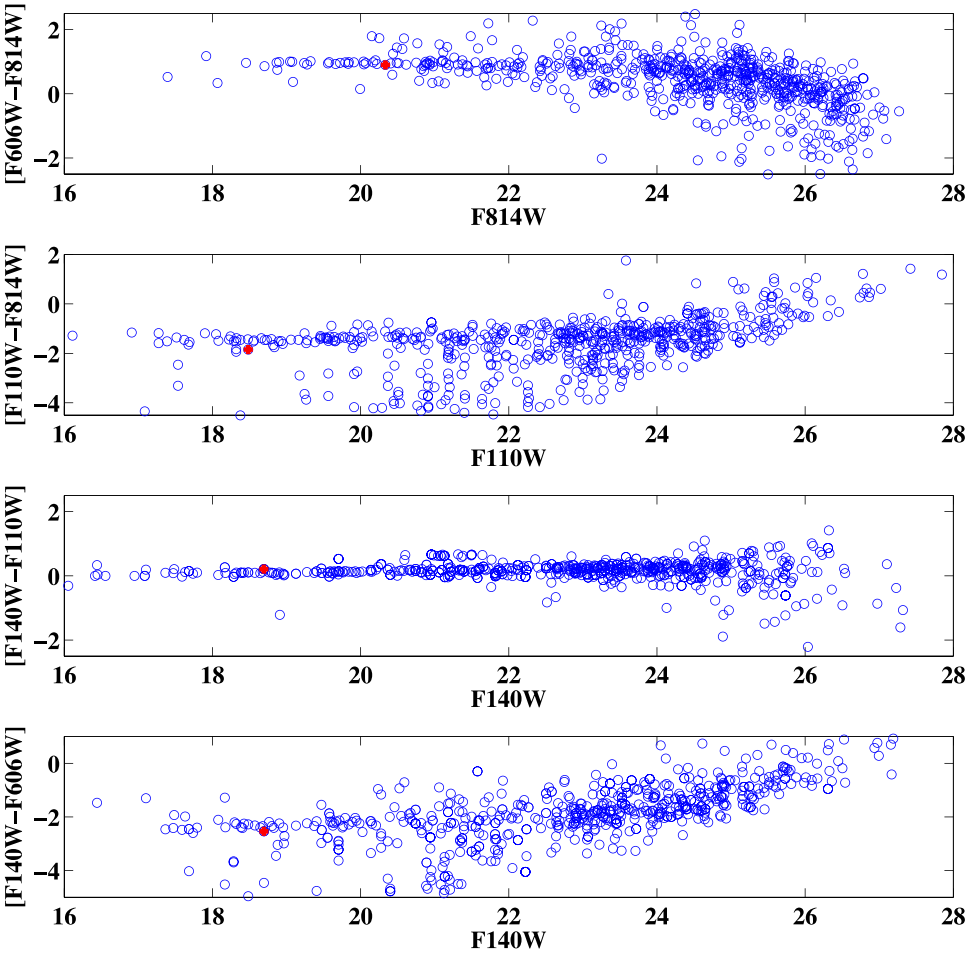

Figure 4. The SG in color–magnitude space. The figure shows four different color–magnitude diagrams from photometric catalogs generated for the central field of M1319. We plot all objects (blue open circles) cross-matched between the different bands in the central $1\farcm5 \times 1\farcm5$ field. The SG (filled red) lies exactly on the top of the easily identifiable cluster-member red sequence, leaving little doubt it is indeed a cluster member. Future spectroscopic redshifts will help to confirm this assumption.

are substantial mass clumps and/or effective ellipticity boosting the critical area and lensing cross section (e.g., Redlich et al. 2012; Zitrin et al. 2013).

Part of the motivation for our work here is to systematically map cluster lenses with archival *HST* imaging, so that the best cosmic telescopes can be designated before the launch of *JWST*. M1319 lies at high ecliptic latitude where the zodiacal IR background is low, which might be beneficial for *JWST* studies of high-redshift galaxies. For $z_s = 15$, for example, we find an effective Einstein radius of $\theta_e(z = 15) \simeq 16''$, enclosing $3.1 \times 10^{13}\ M_\odot$. This is a relatively small lens size compared to other massive clusters (MACS clusters in particular, e.g., Zitrin & Broadhurst 2016, or those selected for the Hubble Frontier Fields program, see Lotz et al. 2016), so that our analysis reveals M1319 is perhaps not in the top class of lensing clusters. Nonetheless, while larger lenses may be more efficient, also somewhat smaller lensing clusters such as M1319 are worth observing, and can usefully magnify faint background sources with—in this case—the advantage that most moderately magnified regions lie well within *HST*'s (and *JWST*'s) near-infrared cameras.

Another main motivation to studying this massive cluster followed the detection of the SG. We now estimate approximately the chances of seeing such a system forming in a galaxy cluster. To form such a symmetric well-aligned SG, the encounter should occur with an impact parameter of the scale of the host's core. This renders the cross section ($\sigma_{\rm SG} = \pi r_{\rm core}^2$) for such a configuration of order kpc^2 (adopting a galaxy core radius of $\sim$0.5–1 kpc). The resulting mean free path before such an event, $l = 1/(n\sigma_{\rm SG})$, where n is the number density of galaxies which we take as $\sim$1000 Mpc^{-3}, a typical thumb number for massive clusters, comes out to be of order $l \sim 1/(10^{-2}) \sim 1000$ Mpc. In contrast, the radius of massive clusters is of order $\sim$1 Mpc, including that of M1319 (Mantz et al. 2010), which means each galaxy has an order of a tenth of a percent to become an SG, in each crossing of the cluster (in general the crossing time is of order Gyr so that only a few crossings per galaxy are expected). To obtain the chance a cluster would produce an SG we need to multiply by the number of galaxies in the cluster for which we take a nominal 1000 galaxies per cluster. However, we only need to account for the fraction of galaxy pairs with low enough relative velocities. We assume a (radial) velocity dispersion of 1000 km s^{-1} and account only for velocities—with respect to the mean velocity—lower than the escape velocity from the SG host which we take as 200 km s^{-1}. This yields to first-order approximation $(200/1000)^3 \sim 1\%$ of the galaxies (or an order of magnitude less, if actually counting only the possible pairs rather then approximating as above). Assuming the dissipation timescale of the shells, i.e., the timeframe in which the shells

can be observed after having formed, is of order Gyr, in total we get that the chance of seeing an SG is of order one in a few dozen to one in a few hundred massive clusters. Note that we neglected the mass distribution of cluster galaxies and did not demand certain mass ratios. Note also that the estimate is susceptible to different assumptions, especially the galaxy core radius (affecting the cross section per galaxy) or escape velocity, that within a reasonable value range can easily change the estimate by an order of magnitude. Overall, this calculation shows why SGs are rare in clusters (note however that we do not refer to the BCG in our estimate here, for which other assumptions may apply). A search for SGs in archival *HST* imaging of other massive clusters would be interesting, to confront and reassess this estimate.

We can exploit our mass model's best-fit *M/L* scaling relation for cluster galaxies to estimate the masses of the SG. Our mass model suggests a total mass of $\sim 1.3 \times 10^{11}\ M_{\odot}$ for the SG system, yielding a mass-to-light ratio of $M/L_B \sim 15$; a typical value for cluster galaxies. The luminosities, or magnitudes, of the SG host (F814W = 20.61 AB) and companion (F814W = 22.50 AB) suggest a minor merger of mass ratio of roughly 10:1. Clearly, this is an upper limit as some stars of the companion are already distributed to the shells, so it was somewhat more massive to begin with than its current luminosity suggests. While we leave detailed modeling of this system to future work, from the mere fact that both the host and progenitor are still observed, and that only two shells are seen, one of them half the distance of the other from the center, it is immediately implied that this a relatively young system compared to the expected merger timescale for this mass ratio (typically of order several Gyr, see for example Boylan-Kolchin et al. 2008; Jiang et al. 2008; Lotz et al. 2008; Ebrova 2013). Indeed, new generations of numerical simulations are now capable of simulating complex SG systems with high resolution (Cooper et al. 2011; Ebrová et al. 2012). Given the rarity of SGs in massive clusters, and our public mass model, it might be interesting to dedicatedly simulate this system in future work.

AZ thanks the reviewer of this work for useful comments. AZ thanks Sirio Belli for his contribution to the Keck/MOSFIRE observations and analysis. AZ is very grateful for a proofread of this manuscript and insightful comments by Ivana Ebrova. While we defer numerically simulating the SG in detail to future work, AZ is indebted to Chris Hayward for help in simulation setup, and acknowledges useful discussions with Margaret Geller, Richard Ellis, Sterl Phinney, Andrew Wetzel, Cameron Hummels, Phil Hopkins, Benny Trakhtenbrot, Dan Stern, Tom Broadhurst, Holland Ford, Re'em Sari, and Harald Ebeling. Comments received from Michal Bilek are appreciated. Principal support for this work was provided by NASA through Hubble Fellowship grant #HST-HF2-51334.001-A awarded by STScI, which is operated by the Association of Universities for Research in Astronomy, Inc. under NASA contract NAS 5-26555. This work is in part based on previous observations made with the NASA/ESA *Hubble Space Telescope*. Data presented herein were obtained at the W.M. Keck Observatory. The authors wish to recognize and acknowledge the very significant cultural role and reverence that the summit of Maunakea has always had within the indigenous Hawaiian community. We are most fortunate to have the opportunity to conduct observations from this mountain.

REFERENCES

Abell, G. O., Corwin, H. G., Jr., & Olowin, R. P. 1989, ApJS, 70, 1
Arp, H. 1966, ApJS, 14, 1
Athanassoula, E., & Bosma, A. 1985, ARA&A, 23, 147
Benítez, N. 2000, ApJ, 536, 571
Bennert, N., Canalizo, G., Jungwiert, B., et al. 2008, ApJ, 677, 846
Bertin, E., & Arnouts, S. 1996, A&AS, 117, 393
Bílek, M., Cuillandre, J.-C., Gwyn, S., et al. 2016, A&A, 588, A77
Boylan-Kolchin, M., Ma, C.-P., & Quataert, E. 2008, MNRAS, 383, 93
Broadhurst, T., Benítez, N., Coe, D., et al. 2005, ApJ, 621, 53
Broadhurst, T., Umetsu, K., Medezinski, E., Oguri, M., & Rephaeli, Y. 2008, ApJL, 685, L9
Canalizo, G., Bennert, N., Jungwiert, B., et al. 2007, ApJ, 669, 801
Coe, D., Benítez, N., Sánchez, S. F., et al. 2006, AJ, 132, 926
Coe, D., Bradley, L., & Zitrin, A. 2015, ApJ, 800, 84
Cooper, A. P., Martínez-Delgado, D., Helly, J., et al. 2011, ApJL, 743, L21
Donahue, M., Ettori, S., Rasia, E., et al. 2016, ApJ, 819, 36
Dupraz, C., & Combes, F. 1986, A&A, 166, 53
Ebeling, H., Edge, A. C., Mantz, A., et al. 2010, MNRAS, 407, 83
Ebrová, I., Jílková, L., Jungwiert, B., et al. 2012, A&A, 545, A33
Ebrova, I. 2013, arXiv:1312.1643
Edwards, L. O. V., Alpert, H. S., Trierweiler, I. L., Abraham, T., & Beizer, V. G. 2016, MNRAS, 461, 230
Fardal, M. A., Guhathakurta, P., Babul, A., & McConnachie, A. W. 2007, MNRAS, 380, 15
Foster, C., Lux, H., Romanowsky, A. J., et al. 2014, MNRAS, 442, 3544
Gu, M., Ho, L. C., Peng, C. Y., & Huang, S. 2013, ApJ, 773, 34
Hennawi, J. F., Dalal, N., Bode, P., & Ostriker, J. P. 2007, ApJ, 654, 714
Hernquist, L., & Quinn, P. J. 1988, ApJ, 331, 682
Hernquist, L., & Spergel, D. N. 1992, ApJL, 399, L117
Irgens, R. J., Lilje, P. B., Dahle, H., & Maddox, S. J. 2002, ApJ, 579, 227
Jiang, C. Y., Jing, Y. P., Faltenbacher, A., Lin, W. P., & Li, C. 2008, ApJ, 675, 1095
Jullo, E., Kneib, J.-P., Limousin, M., et al. 2007, NJPh, 9, 447
Lotz, J. M., Jonsson, P., Cox, T. J., & Primack, J. R. 2008, MNRAS, 391, 1137
Lotz, J. M., Koekemoer, A., Coe, D., et al. 2016, ApJ, submitted (arXiv:1605.06567)
Malin, D. F., & Carter, D. 1980, Natur, 285, 643
Malin, D. F., & Carter, D. 1983, ApJ, 274, 534
Mantz, A., Allen, S. W., Ebeling, H., Rapetti, D., & Drlica-Wagner, A. 2010, MNRAS, 406, 1773
McLean, I. S., Steidel, C. C., Epps, H. W., et al. 2012, Proc. SPIE, 8446, 84460J
Meneghetti, M., Natarajan, P., Coe, D., et al. 2016, MNRAS, submitted (arXiv:1606.04548)
Meneghetti, M., Rasia, E., Vega, J., et al. 2014, ApJ, 797, 34
Merten, J., Meneghetti, M., Postman, M., et al. 2015, ApJ, 806, 4
Monna, A., Seitz, S., Geller, M. J., et al. 2016, MNRAS, submitted (arXiv:1602.08491)
Navarro, J. F., Frenk, C. S., & White, S. D. M. 1996, ApJ, 462, 563
Quinn, P. J. 1984, ApJ, 279, 596
Redlich, M., Bartelmann, M., Waizmann, J.-C., & Fedeli, C. 2012, A&A, 547, A66
Schweizer, F., & Ford, W. K., Jr. 1985, in New Aspects of Galaxy Photometry, Vol. 232 ed. J.-L. Nieto (Berlin: Springer), 145
Schweizer, F., & Seitzer, P. 1988, ApJ, 328, 88
Sereno, M., Jetzer, P., & Lubini, M. 2010, MNRAS, 403, 2077
Sikkema, G., Carter, D., Peletier, R. F., et al. 2007, A&A, 467, 1011
Umetsu, K., Zitrin, A., Gruen, D., et al. 2016, ApJ, 821, 116
Windhorst, R. A., Cohen, S. H., Hathi, N. P., et al. 2011, ApJS, 193, 27
Zitrin, A., & Broadhurst, T. 2016, ApJ, 833, 25
Zitrin, A., Broadhurst, T., Umetsu, K., et al. 2009, MNRAS, 396, 1985
Zitrin, A., Ellis, R. S., Belli, S., & Stark, D. P. 2015a, ApJL, 805, L7
Zitrin, A., Fabris, A., Merten, J., et al. 2015b, ApJ, 801, 44
Zitrin, A., Meneghetti, M., Umetsu, K., et al. 2013, ApJL, 762, L30
Zwicky, F. 1956, ErNW, 29, 344